HHS Public Access

Author manuscript

Biomaterials. Author manuscript; available in PMC 2019 September 01.

Published in final edited form as:

Biomaterials. 2018 September ; 178: 122–133. doi:10.1016/j.biomaterials.2018.06.018.

Multi-channel silk sponge mimicking bone marrow vascular niche for platelet production

Lorenzo Tozzi[a,*], **Pierre-Alexandre Laurent**[b,c,*], **Christian A. Di Buduo**[b,c], **Xuan Mu**[a], **Angelo Massaro**[a], **Ross Bretherton**[a], **Whitney Stoppel**[a], **David L. Kaplan**[a], and **Alessandra Balduini**[a,b,c]

[a]Department of Biomedical Engineering, Tufts University, Medford, MA, USA

[b]Department of Molecular Medicine, University of Pavia, Pavia, Italy

[c]Biotechnology Research Laboratories, IRCCS San Matteo Foundation, Pavia, Italy

Abstract

In the bone marrow, the interaction of progenitor cells with the vasculature is fundamental for the release of blood cells into circulation. Silk fibroin, derived from *Bombyx mori* silkworm cocoons, is a promising protein biomaterial for bone marrow tissue engineering, because of its tunable architecture and mechanical properties, the capacity to incorporate labile compounds without loss of bioactivity and the demonstrated ability to support blood cell formation without premature activation. In this study, we fabricated a custom perfusion chamber to contain a multi-channel lyophilized silk sponge mimicking the vascular network in the bone marrow niche. The perfusion system consisted in an inlet and an outlet and 2 splitters that allowed funneling flow in each single channel of the silk sponge. Computational Fluid Dynamic analysis demonstrated that this design permitted confined flow inside the vascular channels. The silk channeled sponge supported efficient platelet release from megakaryocytes (Mks). After seeding, the Mks localized along SDF-1α functionalized vascular channels in the sponge. Perfusion of the channels allowed the recovery of functional platelets as demonstrated by increased PAC-1 binding upon thrombin stimulation. Further, increasing the number of channels in the silk sponge resulted in a proportional increase in the numbers of platelets recovered, suggesting applicability to scale-up for platelet production. In conclusion, we have developed a scalable system consisting of a multi-

Contact information for correspondence: Alessandra Balduini (alessandra.balduini@tufts.edu), Department of Biomedical Engineering, Tufts University, 4 Colby Street, Medford, MA 02155, USA. Phone: 617-627-2580; Fax: 617-627-3231.

*These authors contributed equally to this study

CONTRIBUTIONS

Lorenzo Tozzi, Pierre-Alexandre Laurent and Christian A. Di Buduo: designed and performed the experiments, analyzed the data and wrote the manuscript; Xuan Mu, Angelo Massaro, Ross Bretherton and Whitney Stoppel: performed the experiments; David L. Kaplan: analyzed the data and edited the manuscript; Alessandra Balduini: conceived the idea, supervised the project, analyzed the data and wrote the manuscript.

DISCLOSURE OF CONFLICTS OF INTEREST

The authors declare no competing financial interests.

channeled silk sponge incorporated in a perfusion chamber that can provide useful technology for functional platelet production *ex vivo*.

INTRODUCTION

The bone marrow (BM) is a complex organ that is responsible for blood cell homeostasis [1]. It is a densely cellularized, gel-like tissue that fills the spongy cavity of bones [2]. The trabecular structure of the cancellous bone, together with the fine mesh of Extracellular Matrix (ECM) proteins provide structural organization, while the extensive BM vascular system constitutes the interface between the hematopoietic tissue and the blood, through which 10^{11}–12^{12} new blood cells are released every day into circulation. The spatial localization of these elements, provides the biochemical and mechanical stimuli for hematopoietic stem cell (HSC) maintenance and differentiation into the different blood lineages [3].

Megakaryocytes (Mks) in the BM are responsible for the continuous production of platelets in the blood [4]. Mks associate with the BM vasculature and extend proplatelets that protrude through the vascular endothelium into the lumen where they release platelets into the bloodstream [5–8]. There are countless human pathologies caused by alterations in platelet production or function, yet for many of these, pathogenesis and the required targeted therapies remain unknown, resulting in palliative treatments [9–11]. Platelet transfusion from donors still constitutes the standard of care for many of these conditions. However, the increasing demand for platelet units together with their extremely short shelf time (~5 days), often results in platelet supply shortages. For this reason, scientific and clinical communities are actively searching for new ways to generate functional platelets *ex vivo* to address clinical needs and for insight into fundamental studies of mechanisms [12, 13]. It is hypothesized that the vascular niche, namely basement membrane components, vascular endothelium and shear, play a pivotal role in directing megakaryopoiesis [6–8, 14].

Engineered BM models that allow *ex vivo* blood cell production hold promise for regenerative medicine. Nevertheless, developing suitable systems for BM engineering presents multiple challenges in terms of material choice, scalability and design [12, 13]. 3D cell cultures are widely used in tissue engineering and regenerative medicine. 3D scaffolds can reproduce the architecture, ECM composition and cellular interactions of native tissues, as well as off extended surface area on which cells adhere and grow, compared to conventional 2D cultures [15, 16]. However, reproducing and maintaining complex tissues *in vitro* in the absence of a vascular system is limited by mass transfer. Bioreactors can be designed to overcome these limitations and provide efficient diffusion of nutrients and oxygen in 3D scaffolds, and can also be used to introduce mechanical stimuli to the engineered tissues [17–19]. Perfusion bioreactors are particularly interesting for BM engineering, since they allow continuous media exchange and enhanced mass transfer through the scaffolds, while also providing flow-induced shear stress to the cells.

Silk fibroin is a natural protein polymer that can be processed into different formats (films, sponges, gels, fibers, microparticles) for many applications, from tissue engineering to drug delivery and regenerative medicine [20–22]. Silk can be processed entirely in water at low

temperature/pressure conditions, which makes it suitable for large-scale batch production [23]. Because of the well-documented biocompatibility, mechanical properties and controlled degradability into non-toxic byproducts, silk-based devices have received approval from the Food and Drug Administration (FDA) for medical and cosmetic applications.

We previously demonstrated that silk-based scaffolds support Mk differentiation and allow functional platelet recovery [24–26]. Building upon our experience, we proposed the rational design of a perfusion bioreactor system that incorporates a BM vascular architecture, mechanical forces and controlled shear (Fig. 1). The advantage of this system is the possibility to control scaffold architecture and properties and to model the flow behavior to obtain maximum platelet yield. In addition, this approach is highly flexible and can be easily scaled for high-volume production of platelets.

MATERIALS AND METHODS

Materials

Bombyx mori silkworm cocoons were supplied by Tajima Shoji Co., Ltd. (Yokohama, Japan). Pharmed tubing was from Cole-Parmer (Vernon Hills, IL, USA). Transfer bags for platelet collection were from Fenwal (Mont Saint Guibert, Belgium). Thrombin was from Sigma Aldrich (Saint Louis, MO, USA and Milan, Italy). Immunomagnetic separation system was from Miltenyi Biotech (Bergisch Gladbach, Germany and Bologna, Italy). Recombinant human thrombopoietin (TPO), interleukin 11 (IL-11), Stromal Derived Factor (SDF)-1α were from Peprotech (London, UK). TruCount tubes and PAC-1 FITC were from Becton Dickinson (S. Jose, CA, USA). 5-(and 6)-Carboxyfluorescein diacetate succinimidyl ester (CFSE) was from BioLegend (London, UK). FITC monoclonal anti-human CD41 (clone HIP8) was from BioLegend. FITC mouse monoclonal anti-human CD61 (clone PM6/13) and PE mouse monoclonal anti-human CD42b (clone HIP1) were from Abcam (Cambridge, UK). Alexa Fluor-conjugated antibodies and Hoechst 33258 were from Life Technologies (Monza, Italy). Anti-human β1-tubulin antibody was kindly provided by Prof. Joseph Italiano Jr.

Silk Solution Preparation

The silk fibroin solution (hereafter referred to as silk) was prepared according to published methods [23]. Silk was extracted from *Bombyx mori* cocoons after sericin removal, by boiling the fibers for 30 minutes in 0.02 M sodium carbonate. The degummed silk fibers were dried in a fume hood for 48 hours and subsequently dissolved in LiBr 9.3 M for 4 hours at 60°C at 25% w/v ratio. The solution was dialyzed using SnakeSkin tubing (3,500 MWCO, Thermo Fisher) for 72 hours, to remove the LiBr. The silk concentration was calculated as the ratio of dry/wet weight of a known volume of silk solution.

Custom molding system fabrication

The custom molding system was designed using AutoCad software (AutoDesk, San Rafael, CA) and machined at Tufts University. The molding system is composed of 3 parts, the base, machined out of corrosion-resistant aluminum (McMaster-Carr, Atlanta, GA), the silk

reservoirs, obtained from polypropylene syringe barrels (BD, Franklin Lakes, NJ) and the lid containing the wire array, fabricated out of Delrin and Teflon-coated stainless-steel wires (0.5 or 1 mm diameter), respectively (McMaster-Carr, Atlanta, GA). A Schematic representation and 3D rendering of the design is reported in Supplementary Fig. 1.

Silk scaffold Preparation

The silk scaffolds were prepared by modifying a previously described method [27, 28], to allow for increased volumes. Briefly, 10 mL of 5% silk solution containing glycerol (0%, 5%, 10%, 20%) and 50 μg/mL collagen type IV (Sigma Aldrich, St Louis, MO), were dispensed for each sponge, in the custom made molding system described above. The solution was incubated for 1 hour at 5°C and then slowly frozen by decreasing the temperature to −45°C at a freezing rate of 0.1°C/minute. The frozen solution was incubated overnight at −45°C and lyophilized for 48h. The lyophilized scaffolds were subsequently autoclaved for 20 min to induce β-sheet formation and stabilize the silk matrix.

Scanning Electron Microscopy imaging

Scanning Electron Microscopy (SEM) imaging was performed on a Zeiss EVO-10MA microscope (Zeiss, Oberkochen, Germany) at 5kV accelerating voltage. Prior to imaging, the samples were thoroughly air-dried in a fume hood for 24h and coated with ~10 nm gold using a SC7620 sputter coater (Quorum Technologies, UK).

Porosity analysis

The silk sponges prepared with different concentration of glycerol (Sigma-Aldrich, St. Louis, MO), were embedded in Optimal Cutting Temperature (OCT) cryosectioning medium (VWR, Radnor, PA). To ensure homogeneous OCT diffusion, the silk sponges were initially immersed in 30% sucrose solution and subjected to several vacuum cycles in order to remove air pockets and allow the solution to fully infiltrate the scaffold. Subsequently, each sample was transferred in an embedding mold and covered in OCT. Vacuum cycles were applied again to allow OCT penetration and eventually, the samples were frozen at −80°C. Each sponge was sectioned in 30 μm slices using a Leica CM 1950 cryotome (Leica, Germany). Samples were dried overnight at 37°C and imaged on a BZ-X700 microscope (Keyence, Japan). For each condition, at least 12 brightfield images were acquired from 4 total sponges obtained from 2 different batches of silk. For pore size calculations, particle count analysis was performed on ImageJ software, setting a threshold to isolate only the single pores (<300 μm diameter), after image conversion to a binary scale. Total porosity was calculated as the white/black area ratio.

Permeability analysis

Permeability analysis was performed based on a custom configured device. Silk sponges doped with glycerol were cut into cylinders of 10×5 mm (diameter x height) by using a biopsy punch. Each cylinder was inserted in a 3 mL Inkredible cartridge (Cellink, Sweden), with matching inner diameter for a tight fitting. The syringes were filled with a constant volume of DI water and connected to the pneumatic-driven extrusion system of the Inkredible 3D printer (Cellink, Sweden). After extrusion on the machine, the time required

to perfuse 3 ml of liquid across the sponge was registered under different pressure values (3, 5, 8, 10, 15, 20, 30, 40, 50 KPa).

The permeability of each sample was calculated according to Darcy's law:

$$Q = \frac{\kappa A(p1 - p2)}{\mu L}$$

Where Q (m^3/s) is the flow rate calculated as described above, κ (m^2) is the sample permeability, A is the sponge cross-section area (m^2), (p1–p2) (Pa) describes the pressure drop, μ (Pa·s) is the liquid viscosity and L is the sample height (m).

Mechanical testing

To assess the mechanical properties of the sponges, unconfined compression tests were conducted on 8 mm diameter cylinders punched from the center of each sponge and equilibrated in water for at least 24h prior to analysis. The samples were analyzed in a TA Instruments RSA3 Dynamic Mechanical Analyzer (TA Instruments, New Castle, DE) through compression at 10% strain per minute between parallel circular plates with the top matching the diameter of the sample. The elastic modulus was calculated from the stress-strain curve slope between 15–25% strain for all samples, with six samples analyzed per condition. This strain window was chosen as it fell within a consistently linear portion of the stress-strain curve for every sample ($R^2 > 0.99$). Frequency dependence of the sponge modulus was also measured at 1% strain over a frequency sweep ranging from 0.1 to 10 Hz.

Bioreactor chamber fabrication

The bioreactor chamber was designed using AutoCAD software (AutoDesk, San Rafael, CA) and machined at Tufts University. All the components were machined using Delrin thermoplastic, which is suitable for use with cell cultures, since it can be autoclaved and does not release toxic byproducts. Stainless steel needles were used to connect the silk sponge channels with the bioreactor inlet/outlet. According to the number of channels in the silk sponge, different pin arrays were used (7, 13 pins).

COMSOL modeling

Finite Element Analysis (FEA) was conducted using the COMSOL Multiphysics 5.2 (COMSOL Inc., MA) to investigate the distribution of shear rate inside silk sponge. The 2D model of the silk sponge cross section was established in COMSOL and meshed into around 1 million triangular elements. We employed Navier-Stokes (1) and Forchheimer-corrected Brinkman equations (2) to describe the free media flow in the channel and the porous media flow in the sponge, respectively.

$$\rho(u \cdot \nabla)u = -\nabla \cdot [\tau + p\delta_{ij}] \quad (1)$$
$$\nabla \cdot u = 0$$

where u is the velocity vector (m/s), τ is the dynamic viscosity (Pa·s), ρ is the fluid's density (kg/m^3), P is the pressure (Pa), and δij is the Kronecker delta function.

$$\nabla p = \mu \nabla^2 u_s - \frac{\mu}{k} u_s \quad (2)$$
$$\nabla \cdot u_s = 0$$

where *k* is the permeability of the porous medium (m^2), u_s denotes the fluid superficial velocity vector (m/s), p is the fluid pressure (Pa), and μ is the effective viscosity in the porous medium (kg/m·s). The permeability and porosity of the silk sponge were obtained from experimental measures, which were 1×10^{-13} m^{-2} and 75%, respectively.

Peripheral blood platelet sample preparation

Human peripheral blood from healthy subjects was purchased from Research Blood Components (Boston, MA, USA). Human peripheral blood platelets were isolated from whole blood that was centrifuged at 200×g for 10 minutes to obtain platelet-rich plasma (PRP). Platelet were finally washed in Tyrode's buffer (134 mM NaCl; 0.34 mM Na_2HPO_4; 2.9 mM KCl; 12 mM $NaHCO_3$; 20 mM HEPES; 5 mM glucose) in the presence of 0.2 U/ml apyrase and 1 μM PGE 1 (Sigma, Milan, Italy) and allowed to rest at room temperature for 1 hour before being used. The morphology of peripheral blood platelets was analyzed by microscopy or flow cytometry, as subsequently described.

Cell Culture

Human umbilical cord blood was collected following physiologic pregnancies and deliveries upon informed consent of the parents. Samples were obtained in accordance with the ethical committee of the IRCCS Policlinico San Matteo Foundation and the principles of the Declaration of Helsinki. Mks were differentiated from human $CD34^+$ hematopoietic stem cells using established protocols [29, 30]. Briefly, $CD34^+$ cells were separated by an immunomagnetic selection technique and cultured for 13 days in serum-free medium (StemSpan, STEMCELL Technologies, Canada) supplemented with 10 ng/mL TPO, IL-11, 1% penicillin-streptomycin (P/S) and 1% L-glutamine, at 37°C in a 5% CO_2 incubator.

Megakaryocyte seeding and sponge perfusion for *ex vivo* platelet production

The channels of a silk sponge, sterilized by autoclaving, were coated with silk hydrogel (6% w/v) obtained by sonication of silk solution (4°C, 2 × 3 0 sec, amplitude 40%), and supplemented with human SDF-1α (300 ng/ml). The sponge was left to dry vertically for 2 hours under a sterile hood, and then mounted in the core of the device sealed by the bottom. The sponge was rehydrated first with Phosphate-Buffered Saline (PBS), then with Stem Span medium supplemented with 10 ng/mL TPO, 1% P/S. At day 12 of differentiation, ~1.5×10^6 $CD41^+CD42b^+$ cord-blood derived Mks were seeded within the 3D scaffold drop-by-drop, on the surface of the scaffolds, to ensure homogeneous seeding. Finally, the full bioreactor was assembled, taking care to fill any empty volume with medium. After 36 hours of incubation at 37°C and 5% CO_2, the bioreactor was connected to a syringe containing

DMEM with 1% penicillin/streptomycin and L-glutamine 2 mM, which was injected for 6 hours at a flow rate of 10 μL/min using a syringe pump (PHD 2000, Harvard Apparatus, Holliston, MA). The released platelets were collected in a transfusion bag containing ACD as anticoagulant. A schematic representation including details for the different steps of Mk seeding and sponge perfusion is reported in Supplementary Fig. 2.

Immunofluorescence microscopy

For analysis of Mk maturation and proplatelet formation, cells at the end of differentiation were allowed to adhere overnight, at 37°C and 5% CO_2, on glass coverslips previously coated with 25 μg/ml type IV collagen and then fixed in 4% PFA [31]. Proplatelet forming Mks were identified as cells displaying long filamentous structure ending with platelet-sized tips [32].

All samples were permeabilized with 0.1% Triton X-100 for 5 minutes and blocked with 5% BSA for 30 minutes, at room temperature. In order to visualize microtubules organization samples were probed with anti-β1-tubulin (1:1000) for 1 hour at room temperature and then immersed in Alexa Fluor® 594 secondary antibody (1:500) for 2 hours at room temperature. Nuclei were stained with Hoechst 33258 (1:10000) for 5 minutes. Platelets were fixed and stained by same protocol. All samples were mounted onto glass slides with ProLong Gold antifade reagent (Invitrogen, Milan, Italy) and then imaged by an Olympus BX51 fluorescence microscope (Olympus Deutschland GmbH, Hamburg, Germany).

For 3D immunofluorescence imaging Mks were labeled with 0.5 μM of 5-(and 6)-carboxyfluorescein diacetate succinimidyl ester (CFSE) for 15 minutes, at room temperature and washed 2 times with culture media, before being dispensed into silk scaffold [26]. Samples were imaged by an Olympus FluoView FV10i confocal laser-scanning microscope (Olympus, Tokyo, Japan). For silk scaffolds imaging we took advantage of silk auto-fluorescence in UV light, silk fluorescence was further brighten by staining with Hoechst 33258 (1:10000) for 5 minutes. 3D reconstruction and image processing was performed using ImageJ software.

Flow cytometry analysis

Flow cytometry settings for analysis of *ex vivo* generated platelets were established, as previously described [26], using the same forward and side scatter pattern as human peripheral blood platelets. Platelets were identified as $CD61^+$, $CD41^+$ and $CD42b^+$ events. Isotype controls were used as a negative control to exclude non-specific background signal. Platelet number was calculated using a TruCount bead standard. For the analysis of platelet functionality, platelets were activated with 3 U/mL thrombin for 15 minutes at 37°C. Non-stimulated pla telets were used to gate for non-activated platelets. Cells exhibiting PAC-1 binding were considered functional activated platelets. All samples were acquired with a Beckman-Coulter Navios flow cytometer. Off-line data analysis was performed using Beckman-Coulter Navios software package.

Statistics

Statistical analysis was performed on GraphPad Prism software (GraphPad, LaJolla, CA). To assess statistical significance, we used a one-way ANOVA and Tukey post hoc test for multiple comparisons.

Availability of data and materials

All the datasets supporting the conclusions of this article are included within the article (and its additional files).

RESULTS

Large volume channeled scaffolds fabrication

Large-volume channeled scaffolds were obtained by slowly freezing 10 mL of 5% silk solution, at a controlled rate of 0.1°C/minute and subsequent lyop hilization (Fig. 2A). This resulting sponge had an average volume of 8.7±0.1 cm^3 (Fig. 2B **and** Supplementary Fig. 3). The sponges were autoclaved for 20 min at 121°C in order to stabilize silk seco ndary structure and make them insoluble in water, as previously described [28]. The controlled slow-freezing rate protocol allowed for homogeneous ice crystals formation from the bottom to the top of the scaffold, without creating freezing fronts and resulted in a highly homogeneous porous structure across the whole scaffold (Fig. 2D). A custom-made molding system was built that allowed incorporation of a channel array in the scaffolds, with tunable geometry and size (Supplementary Fig. 1). The molding system was composed of an aluminum base, which improved heat exchange between the lyophilizer shelf and the silk solution. Polypropylene barrels were adapted on top of the aluminum base as silk reservoirs. Finally, a Delrin lid that contained the circular wire arrays was machined with different wire sizes and geometries (Fig. 2B) to allow the incorporation of up to 61 channels of 0.5 or 1 mm diameter for each scaffold (Fig. 2C). The scaffold architecture was not altered by the wire array, maintaining homogeneous porosity in close proximity to the channels (Fig. 2Di). Importantly, the channel lumen was separated from the bulk of the scaffold by an open-pore interface that resembles the discontinuous and fenestrated structure of BM capillaries (Fig. 2Dii).

Silk scaffold characterization

In order to allow homogeneous cell seeding across the sponge volume, scaffolds should display interconnected pores, large enough to allow cell infiltration and permeable to allow rapid diffusion of media, nutrients and oxygen from the perfused channels to the bulk. Glycerol is a non-toxic humectant, widely used in the pharmaceutical formulations and previously employed in combination with silk biomaterials, to improve the physico-chemical properties. Silk sponges, containing increasing concentrations of glycerol (0, 5, 10, 20%) were prepared as described earlier in order to characterize the effect of glycerol on porosity, permeability and mechanical properties. The addition of glycerol improved scaffold volume and shape retention after lyophilization and autoclaving, compared to silk only sponges (Supplementary Fig. 3), confirming previously published data [33].

Porosity measurements were performed through a sample sectioning/imaging technique. Briefly, each sponge was cryosectioned into multiple 30 μm sections and imaged under a standard bright-field microscope. The acquired images were processed to convert them to a binary scale and the pore cross-section area was automatically extrapolated (Fig. 3A and 3B). The addition of 10% and 20% (w/w) glycerol slightly decreased the overall pore sizes, however, the calculated differences are not significant (126±3.7 μm, 122±4.8 μm, 116±7.5 μm, 117±4.9 μm for 0%, 5%, 10%, 20% glycerol, respectively). The addition of 10% and 20% glycerol yielded more interconnected pores as shown by SEM analysis (Fig. 3A), while no differences in total porosity were observed among samples (Fig. 3C).

Scaffold permeability was measured through a pneumatic-driven perfusion setup and calculated based on the linear relationship between fluid velocity and pressure difference across the sponge, according to Darcy's law. The permeability is related to multiple factors including the pore size, pore interconnectivity of the scaffolds and the material properties. Indeed, a glycerol concentration-dependent effect on sponge permeability was observed. In particular, sponges fabricated with the addition of 20% glycerol, displayed the highest permeability values, while silk only sponges the lowest (Fig. 3D **and** Supplementary Fig. 4).

The characterization of mechanical properties was performed by unconfined compression tests of wet sponges and the elastic modulus was calculated from the stress-strain curve slope between 15–25% strain. No differences between the different conditions were observed, with a Young's modulus around 90±52 kPa (mean±SD) for all scaffolds (Fig. 3E). It is important to note that these values are within an order of magnitude comparable to *in vivo* BM tissue [34]. Silk scaffolds prepared with 20% glycerol were chosen for all the subsequent experiments, due to the increased permeability and pore interconnectivity.

Bioreactor design and flow simulations

A custom perfusion chamber was designed and fabricated to contain the silk scaffolds and allow perfusion of the channels. As shown in the schematic of the bioreactor design in Fig. 4A and 4B, the system consists of 5 separate components: the central chamber that contains the sponge, the inlet and outlet that connect the chamber to the perfusion system and 2 flow splitters to connect the sponge to the inlet and outlet and allow flow to funnel into each single channel. This design permits better control on flow dynamics inside the scaffold, avoiding "edge flows" between the scaffold and the bioreactor wall. To verify the flow characteristics, Computational Fluid Dynamic analysis was utilized, based on scaffold geometry and physical properties described above. In particular, scaffold porosity and permeability were determined to reliably simulate fluid behavior to extrapolate flow velocity and shear values. According to the material characterization above, we set a porosity value of 75% and a permeability value of 10^{-13} m^2. The scaffold geometry was based on the large volume (≈7,850 mm^3) silk sponges described above. To evaluate the impact of channel number and distribution on the flow properties, we compared 7 and 13 channels conditions. Due to the different flow condition, two equations, Navier-Stokes (1) and Forchheimer-corrected Brinkman equations (2), were employed to describe the free media flow in the channel and across the sponge, respectively. Fig. 5A and 5C show the shear-rate profiles within the 7 and 13 channels scaffolds, respectively, at steady-state flow conditions only a

central section of each scaffold is shown in the simulation, assuming symmetric flow and homogeneous properties within the silk sponge. The results show that the flow was almost entirely confined within the channels, which display a homogeneous flow profile across the whole length (Fig. 5), while negligible flow was observed within the scaffold bulk. This flow pattern creates a sharp transition in shear values between the channels and the silk sponge (Fig. 5B and 5D). As expected, an almost linear decrease in shear values was observed between the 7 and 13 channel geometries at equivalent input flow velocity (Fig. 5B and 5D).

Ex vivo platelet production from human megakaryocytes

To validate the biocompatibility of the device and the efficiency of *ex vivo* platelet production, we took advantage of our well characterized protocol for differentiating mature Mks from cord blood-derived progenitors. Fig. 6Ai, ii and 6B demonstrate that after 13 days of differentiation $CD41^{+}CD42b^{+}$ polyploid Mks were able to form proplatelets *in vitro*. In order to collect platelets, Mks were seeded within 7 or 13 channels silk sponges mounted inside the perfusion chamber and cultured for 36 hours before perfusion. Medium was perfused at a low flow rate (10 μl/min) for 6 hours, to limit the total collected volume and avoid excessive platelet dilution (Fig. 6C). Confocal microscopy imaging of the 3D culture before starting perfusion demonstrated that the high pore interconnectivity of the silk scaffold supported Mk distribution next to the SDF-1α-coated channels (Fig. 6Di, ii).

After perfusion, *ex vivo* collected platelets were stained with anti-CD61, anti-CD41 and anti-CD42b antibodies and analyzed by flow cytometry to confirm the expression of human peripheral blood platelet receptors. As shown in Fig. 7A, targeted population expressed all these classical platelet surface markers, with a median number of 0.4×10^{6} platelets (range: $0.2–1\times10^{6}$) collected after perfusion of the 7 channels sponge *versus* 2×10^{6} platelets (range: $0.8–4.5\times10^{6}$) collected after perfusion of the 13 channels sponge (Fig. 7B). The analysis of platelet morphology by epifluorescence microscopy revealed the presence of β1-tubulin positive barbell-shaped proplatelets, which are correlated to the final step of thrombopoiesis occurring in the bloodstream (Fig. 7C), and typical discoid platelets exhibiting well-shaped submembranous microtubule rings, as found in the peripheral blood (Fig. 7C, Supplementary Fig. 5).

Finally, platelet functionality was evaluated through the study of the conformation changes of the integrin αIIbβ3 (CD41/61) reflecting the platelet activation. Samples were incubated with FITC-conjugated PAC-1 which specifically binds the activated conformation of CD41, and then activated with thrombin (3 U/ml) for 15 minutes at 37°C. $CD42b^{+}$ events exhibiting PAC-1 binding were considered functional activated platelets. Platelets exhibiting an activated CD41 conformation after thrombin-induced activation represented 60±5% of the population, confirming that the generated platelets were physiologically functional (Fig. 7D).

DISCUSSION

In this paper, we propose a strategy to scale up our recently published silk sponge system mimicking the spongy structure of the BM [24, 25], for *ex vivo* production of functional platelets. We developed a channeled silk sponge by slowly freezing a 5% silk solution at a

controlled rate with subsequent lyophilization. A custom-made molding system allowed the incorporation of different numbers of channels in the silk sponges, without altering the scaffold architecture. It has been demonstrated that the stiffness of the BM environment impacts Mk function, with softer substrates determining an increase in platelet release and proplatelet formation [24, 31, 35–37]. Accordingly, our lyophilized sponge displayed soft mechanics resembling BM elasticity [34], effectively supporting Mk differentiation and platelet release. The ECM composition of the BM plays a pivotal role in regulating Mk behavior [14, 38] and basement membrane components have been shown to support proplatelet formation and platelet release [24, 29]. Consistently, functionalization of the lyophilized silk sponge with type IV collagen supported proplatelet formation by the Mks seeded in the system and the collection of well-shaped platelets showing ability to respond to physiologic stimuli of hemostasis.

The role of shear forces and flow in platelet generation *ex vivo* have been explored in previous work that attempted to mimic the physiology of the BM by a two-dimensional flow bioreactor [39] or to induce platelet shedding by exposing Mks to high shear in a multi-pillar flow chamber [40]. Additionally microfluidic bioreactors have been developed to recapitulate BM hemodynamic vascular shear stress for platelet generation [41]. In a departure from these previous studies and models [24–26], we demonstrated that lyophilized silk sponges can be manipulated to incorporate multiple vascular channels that mimic the BM micro-vascular network better, thus increasing the contact between Mks and the vasculature and the release of platelets in circulation. These prior solutions referenced above also represented an elegant engineering approach to produce platelets, however they process very small volumes at a time. Our lyophilized silk sponges allowed us to control the shear conditions in the perfused channels, to better reproduce the flow dynamics of bone marrow capillaries, while retaining the possibility to process large volumes of cells as required for clinical translation. In fact, the high porosity and the 3D architecture of our silk scaffolds provided a large surface area for cell attachment, thus allowing the culture of higher cell numbers in smaller volumes of media. In addition, the possibility to control scaffold geometry, as well as material properties, allow us to control the shear conditions in the perfused channels, to better reproduce the flow dynamics of bone marrow capillaries. To this end, detailed material characterization, together with computational flow dynamics analysis demonstrated to be instrumental to understand the flow behavior in our bioreactor system and could be use in the future to optimize the system. Finally, the silk scaffolds in this manuscript also meet the requirements for large-scale production in terms of ease of fabrication and reasonable costs. Indeed, the single-step freeze/dry processing allows for rapid fabrication of large batches of scaffolds in a single cycle, with high reproducibility.

Despite the fact that a direct comparison of the platelet yield between the different approaches described would not be entirely accurate, due to the different cell sources and analysis parameters employed between different labs, the approach described in this paper displayed a greater potential to generate platelet numbers compared to our previous bioreactor [24]. In fact, the number of Mks seeded for each sponge was set to about 1.5 million/sponge, which corresponds to about 190 Mk/mm^3 (considering the average volume of the sponge, Supplementary Fig. 3). While the ratio of Mk for scaffold volume in our previously published models was about 550 Mk/mm^3. According to these calculations, the

platelet yield with the first version of our bioreactor was about 3,600 Plt/Mk/mm^3, while the approach presented in the present work yielded about 23,600 Plt/Mk/mm^3, which represents a six folds increase in efficiency.

Overall, these data demonstrated that the more closely one mimics the BM vascular niche, in terms of physical and biochemical parameters, the better the yield of platelets is.

Nevertheless, more research is needed to further improve the platelet yield. This will entail the optimization of the scaffold and perfusion parameters, as well as the exploitation of different cell sources, which are more efficient and scalable, such as pluripotent stem cell-derived Mks [42, 43].

In conclusion, we developed a multi-channel vascular system to reproduce the BM vascular niche to support platelet shedding by human Mks into flow. The versatility of the silk biomaterials we employed and our system design allows for multiple applications of this bioreactor from basic studies to scale-up *ex vivo* platelet production.

Supplementary Material

Refer to Web version on PubMed Central for supplementary material.

Acknowledgments

The authors would like to thank Dr. Rita Maccario and Dr. Margherita Massa for technical assistance with the flow cytometry analysis; Dr. Cesare Perotti for supplying human cord blood; Prof. Joseph Italiano for providing β1-tubulin antibody. This paper was supported by Cariplo Foundation (2013-0717), ERA-Net for Research Programmes on Rare Diseases (EUPLANE), US National Institutes of Health (R01 EB016041-02), European Haematology Association (EHA) and Japanese Society of Hematology (JSH) fellowship and Ministry of Foreign Affairs and International Cooperation, H2020-FETOPEN-1-2016-2017-SilkFUSION. Christian A. Di Buduo fellowship was funded by Collegio Ghislieri, Pavia, progetto “Progressi in Biologia e Medicina”. The funders had no role in study design, data collection and analysis, decision to publish, or preparation of the manuscript.

References

1. Morrison SJ, Scadden DT. The bone marrow niche for haematopoietic stem cells. Nature. 2014; 505(7483):327–34. [PubMed: 24429631]
2. Travlos GS. Normal structure, function, and histology of the bone marrow. Toxicol Pathol. 2006; 34(5):548–65. [PubMed: 17067943]
3. Wang LD, Wagers AJ. Dynamic niches in the origination and differentiation of haematopoietic stem cells. Nat Rev Mol Cell Biol. 2011; 12(10):643–55. [PubMed: 21886187]
4. Malara A, Abbonante V, Di Buduo CA, Tozzi L, Currao M, Balduini A. The secret life of a megakaryocyte: emerging roles in bone marrow homeostasis control. Cellular and Molecular Life Sciences. 2015; 72(8):1517–1536. [PubMed: 25572292]
5. Italiano JE, Shivdasani RA. Megakaryocytes and beyond: the birth of platelets. J Thromb Haemost. 2003; 1(6):1174–82. [PubMed: 12871316]
6. Avecilla ST, Hattori K, Heissig B, Tejada R, Liao F, Shido K, Jin DK, Dias S, Zhang F, Hartman TE, Hackett NR, Crystal RG, Witte L, Hicklin DJ, Bohlen P, Eaton D, Lyden D, de Sauvage F, Rafii S. Chemokine-mediated interaction of hematopoietic progenitors with the bone marrow vascular niche is required for thrombopoiesis. Nat Med. 2004; 10(1):64–71. [PubMed: 14702636]
7. Junt T, Schulze H, Chen Z, Massberg S, Goerge T, Krueger A, Wagner DD, Graf T, Italiano JE, Shivdasani RA, von Andrian UH. Dynamic visualization of thrombopoiesis within bone marrow. Science. 2007; 317(5845):1767–70. [PubMed: 17885137]

8. Zhang L, Orban M, Lorenz M, Barocke V, Braun D, Urtz N, Schulz C, von Bruhl ML, Tirniceriu A, Gaertner F, Proia RL, Graf T, Bolz SS, Montanez E, Prinz M, Muller A, von Baumgarten L, Billich A, Sixt M, Fassler R, von Andrian UH, Junt T, Massberg S. A novel role of sphingosine 1-phosphate receptor S1pr1 in mouse thrombopoiesis. The Journal of experimental medicine. 2012; 209(12):2165–81. [PubMed: 23148237]

9. Balduini CL, Savoia A, Seri M. Inherited thrombocytopenias frequently diagnosed in adults. J Thromb Haemost. 2013; 11(6):1006–19. [PubMed: 23510089]

10. Malara A, Abbonante V, Di Buduo CA, Tozzi L, Currao M, Balduini A. The secret life of a megakaryocyte: emerging roles in bone marrow homeostasis control. Cell Mol Life Sci. 2015; 72(8):1517–36. [PubMed: 25572292]

11. Balduini CL, Pecci A, Noris P. Diagnosis and management of inherited thrombocytopenias. Semin Thromb Hemost. 2013; 39(2):161–71. [PubMed: 23397552]

12. Di Buduo CA, Kaplan DL, Balduini A. In vitro generation of platelets: Where do we stand? Transfus Clin Biol. 2017; 24(3):273–276. [PubMed: 28669522]

13. Balduini A, Di Buduo CA, Kaplan DL. Translational approaches to functional platelet production ex vivo. Thrombosis and haemostasis. 2016; 115(2):250–6. [PubMed: 26353819]

14. Malara A, Currao M, Gruppi C, Celesti G, Viarengo G, Buracchi C, Laghi L, Kaplan DL, Balduini A. Megakaryocytes contribute to the bone marrow-matrix environment by expressing fibronectin, type IV collagen, and laminin. Stem cells. 2014; 32(4):926–37. [PubMed: 24357118]

15. Ou KL, Hosseinkhani H. Development of 3D in vitro technology for medical applications. Int J Mol Sci. 2014; 15(10):17938–62. [PubMed: 25299693]

16. Bhatia SN, Ingber DE. Microfluidic organs-on-chips. Nat Biotechnol. 2014; 32(8):760–72. [PubMed: 25093883]

17. Lovett M, Lee K, Edwards A, Kaplan DL. Vascularization strategies for tissue engineering. Tissue Eng Part B Rev. 2009; 15(3):353–70. [PubMed: 19496677]

18. Bergemann C, Elter P, Lange R, Weißmann V, Hansmann H, Klinkenberg ED, Nebe B. Cellular Nutrition in Complex Three-Dimensional Scaffolds: A Comparison between Experiments and Computer Simulations. Int J Biomater. 2015; 2015:584362. [PubMed: 26539216]

19. Caddeo S, Boffito M, Sartori S. Tissue Engineering Approaches in the Design of Healthy and Pathological In Vitro Tissue Models. Front Bioeng Biotechnol. 2017; 5:40. [PubMed: 28798911]

20. Omenetto FG, Kaplan DL. New opportunities for an ancient material. Science. 2010; 329(5991): 528–31. [PubMed: 20671180]

21. Kluge JA, Li AB, Kahn BT, Michaud DS, Omenetto FG, Kaplan DL. Silk-based blood stabilization for diagnostics. Proceedings of the National Academy of Sciences of the United States of America. 2016; 113(21):5892–7. [PubMed: 27162330]

22. Lovett M, Eng G, Kluge JA, Cannizzaro C, Vunjak-Novakovic G, Kaplan DL. Tubular silk scaffolds for small diameter vascular grafts. Organogenesis. 2010; 6(4):217–24. [PubMed: 21220960]

23. Rockwood DN, Preda RC, Yucel T, Wang X, Lovett ML, Kaplan DL. Materials fabrication from Bombyx mori silk fibroin. Nature protocols. 2011; 6(10):1612–31. [PubMed: 21959241]

24. Di Buduo CA, Wray LS, Tozzi L, Malara A, Chen Y, Ghezzi CE, Smoot D, Sfara C, Antonelli A, Spedden E, Bruni G, Staii C, De Marco L, Magnani M, Kaplan DL, Balduini A. Programmable 3D silk bone marrow niche for platelet generation ex vivo and modeling of megakaryopoiesis pathologies. Blood. 2015; 125(14):2254–64. [PubMed: 25575540]

25. Di Buduo CA, Currao M, Pecci A, Kaplan DL, Balduini CL, Balduini A. Revealing Eltrombopag's promotion of human megakaryopoiesis through AKT/ERK-dependent pathway activation. Haematologica. 2016; 101(12):1479–1488. [PubMed: 27515246]

26. Di Buduo CA, Soprano PM, Tozzi L, Marconi S, Auricchio F, Kaplan DL, Balduini A. Modular flow chamber for engineering bone marrow architecture and function. Biomaterials. 2017; 146:60–71. [PubMed: 28898758]

27. Rnjak-Kovacina J, Wray LS, Golinski JM, Kaplan DL. Arrayed Hollow Channels in Silk-based Scaffolds Provide Functional Outcomes for Engineering Critically-sized Tissue Constructs. Adv Funct Mater. 2014; 24(15):2188–2196. [PubMed: 25395920]

28. Rnjak-Kovacina J, Wray LS, Burke KA, Torregrosa T, Golinski JM, Huang W, Kaplan DL. Lyophilized Silk Sponges: A Versatile Biomaterial Platform for Soft Tissue Engineering. ACS Biomater Sci Eng. 2015; 1(4):260–270. [PubMed: 25984573]
29. Balduini A, Pallotta I, Malara A, Lova P, Pecci A, Viarengo G, Balduini CL, Torti M. Adhesive receptors, extracellular proteins and myosin IIA orchestrate proplatelet formation by human megakaryocytes. Journal of thrombosis and haemostasis: JTH. 2008; 6(11):1900–7. [PubMed: 18752571]
30. Abbonante V, Di Buduo CA, Gruppi C, Malara A, Gianelli U, Celesti G, Anselmo A, Laghi L, Vercellino M, Visai L, Iurlo A, Moratti R, Barosi G, Rosti V, Balduini A. Thrombopoietin/TGF-β1 Loop Regulates Megakaryocyte Extracellular Matrix Component Synthesis. Stem Cells. 2016; 34(4):1123–33. [PubMed: 26748484]
31. Abbonante V, Di Buduo CA, Gruppi C, De Maria C, Spedden E, De Acutis A, Staii C, Raspanti M, Vozzi G, Kaplan D, Moccia F, Ravid K, Balduini A. A new path to platelet production through matrix sensing. Haematologica. 2017; 102(7):1150–1160. [PubMed: 28411253]
32. Di Buduo CA, Alberelli MA, Glembostky AC, Podda G, Lev PR, Cattaneo M, Landolfi R, Heller PG, Balduini A, De Candia E. Abnormal proplatelet formation and emperipolesis in cultured human megakaryocytes from gray platelet syndrome patients. Sci Rep. 2016; 6:23213. [PubMed: 26987485]
33. Brown JE, Moreau JE, Berman AM, McSherry HJ, Coburn JM, Schmidt DF, Kaplan DL. Shape Memory Silk Protein Sponges for Minimally Invasive Tissue Regeneration. Adv Healthc Mater. 2017; 6(2)
34. Jansen LE, Birch NP, Schiffman JD, Crosby AJ, Peyton SR. Mechanics of intact bone marrow. J Mech Behav Biomed Mater. 2015; 50:299–307. [PubMed: 26189198]
35. Shin JW, Swift J, Spinler KR, Discher DE. Myosin-II inhibition and soft 2D matrix maximize multinucleation and cellular projections typical of platelet-producing megakaryocytes. Proc Natl Acad Sci U S A. 2011; 108(28):11458–63. [PubMed: 21709232]
36. Malara A, Gruppi C, Pallotta I, Spedden E, Tenni R, Raspanti M, Kaplan D, Tira ME, Staii C, Balduini A. Extracellular matrix structure and nano-mechanics determine megakaryocyte function. Blood. 2011; 118(16):4449–53. [PubMed: 21828129]
37. Aguilar A, Pertuy F, Eckly A, Strassel C, Collin D, Gachet C, Lanza F, Leon C. Importance of environmental stiffness for megakaryocyte differentiation and proplatelet formation. Blood. 2016; 128(16):2022–2032. [PubMed: 27503502]
38. Malara A, Gruppi C, Rebuzzini P, Visai L, Perotti C, Moratti R, Balduini C, Tira ME, Balduini A. Megakaryocyte-matrix interaction within bone marrow: new roles for fibronectin and factor XIII-A. Blood. 2011; 117(8):2476–83. [PubMed: 21131589]
39. Nakagawa Y, Nakamura S, Nakajima M, Endo H, Dohda T, Takayama N, Nakauchi H, Arai F, Fukuda T, Eto K. Two differential flows in a bioreactor promoted platelet generation from human pluripotent stem cell-derived megakaryocytes. Exp Hematol. 2013; 41(8):742–8. [PubMed: 23618622]
40. Blin A, Le Goff A, Magniez A, Poirault-Chassac S, Teste B, Sicot G, Nguyen KA, Hamdi FS, Reyssat M, Baruch D. Microfluidic model of the platelet-generating organ: beyond bone marrow biomimetics. Sci Rep. 2016; 6:21700. [PubMed: 26898346]
41. Thon JN, Mazutis L, Wu S, Sylman JL, Ehrlicher A, Machlus KR, Feng Q, Lu S, Lanza R, Neeves KB, Weitz DA, Italiano JE. Platelet bioreactor-on-a-chip. Blood. 2014; 124(12):1857–67. [PubMed: 25606631]
42. Moreau T, Evans AL, Vasquez L, Tijssen MR, Yan Y, Trotter MW, Howard D, Colzani M, Arumugam M, Wu WH, Dalby A, Lampela R, Bouet G, Hobbs CM, Pask DC, Payne H, Ponomaryov T, Brill A, Soranzo N, Ouwehand WH, Pedersen RA, Ghevaert C. Large-scale production of megakaryocytes from human pluripotent stem cells by chemically defined forward programming. Nat Commun. 2016; 7:11208. [PubMed: 27052461]
43. Nakamura S, Takayama N, Hirata S, Seo H, Endo H, Ochi K, Fujita K, Koike T, Harimoto K, Dohda T, Watanabe A, Okita K, Takahashi N, Sawaguchi A, Yamanaka S, Nakauchi H, Nishimura S, Eto K. Expandable megakaryocyte cell lines enable clinically applicable generation of platelets from human induced pluripotent stem cells. Cell Stem Cell. 2014; 14(4):535–48. [PubMed: 24529595]

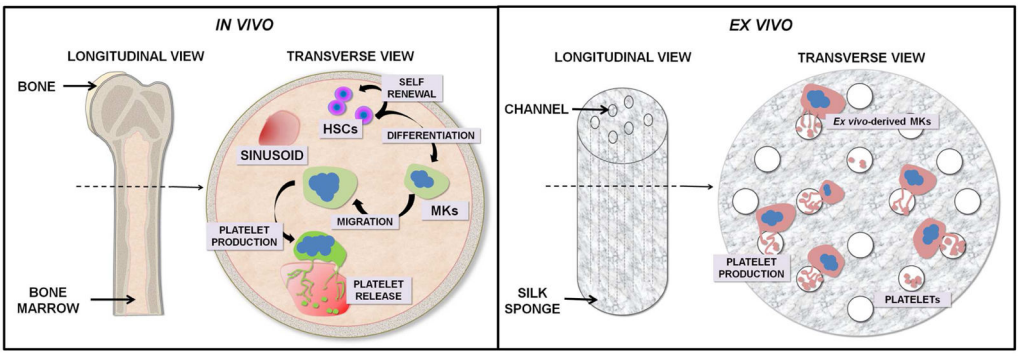

Fig. 1.

Schematic representation of *in vivo* megakaryopoiesis *VS ex vivo* modeling using the multichannel silk sponge. Bone marrow is a spongy tissue composed by a network of sinusoids and ECMs. Within this context hematopoietic stem cells (HSCs) undergo self-renewal as well as differentiation into all committed lineages. Specifically, thrombopoietin (TPO) promotes differentiation into megakaryocytes (Mks) that are in close contact with sinusoids, where they extend multiple long pseudopods, called proplatelets that assemble platelets at their terminal ends. The release of mature platelets can be attributed to blood hydrodynamics that promote their final shedding. In order to mimic these functions, we designed a multi-channel silk sponge to allow Mk culture and perfusion of medium in order to recover *ex vivo*-released platelets.

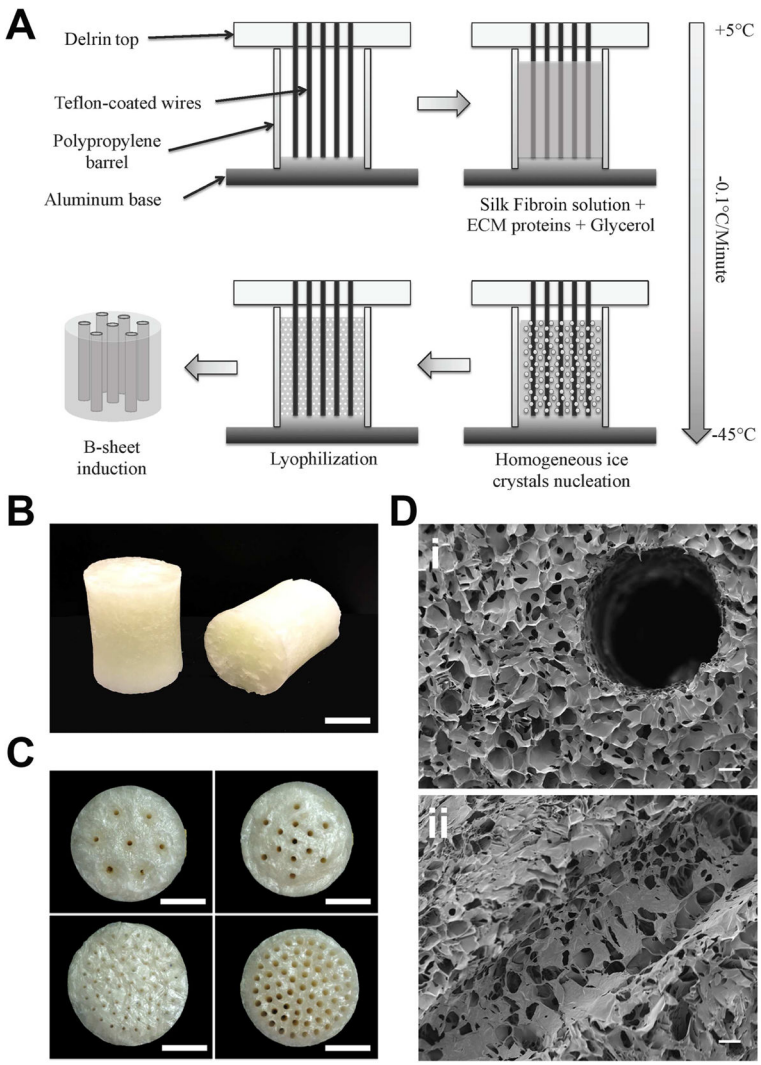

Fig. 2.

Silk sponge fabrication schematics (A). Representative images of 10 mL silk sponges, scale bar = 1 cm (B). Representative images of 7×1 mm channels, 13×1 mm channels, 61×0.5 mm channels and 61×1 mm channels sponges (top left to bottom right respectively, scale bar = 1 cm) (C). SEM micrographs showing the porous structure around (top panel) and inside the channels (bottom panel), scale bar = 100 μm (D).

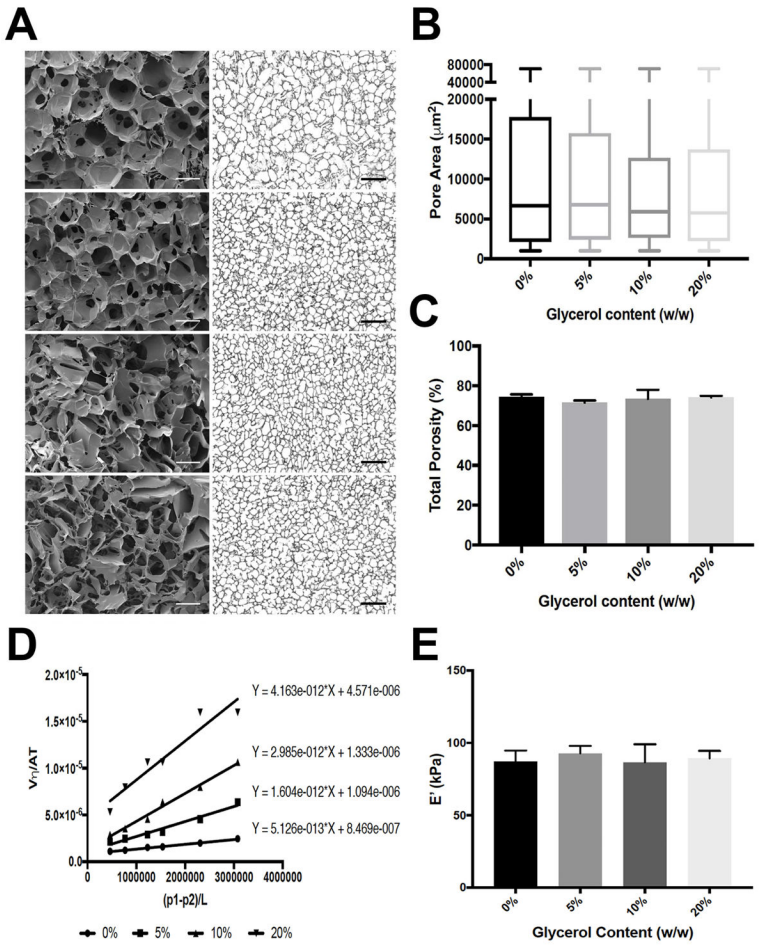

Fig. 3.

SEM micrographs (left) and bright field images (right) showing sponge porosity at increasing glycerol concentrations (scale bar = 100 μm and 500 μm respectively) (A). Quantification of the pore size diameter (B) and total porosity (C) as a function of glycerol content. Graph showing the linear fitting of the permeability measurements. The permeability value (m^2), calculated as the slope of the fitting line is reported next to each data set (D). Young's modulus representation of the silk scaffolds prepared with increasing glycerol concentration (E).

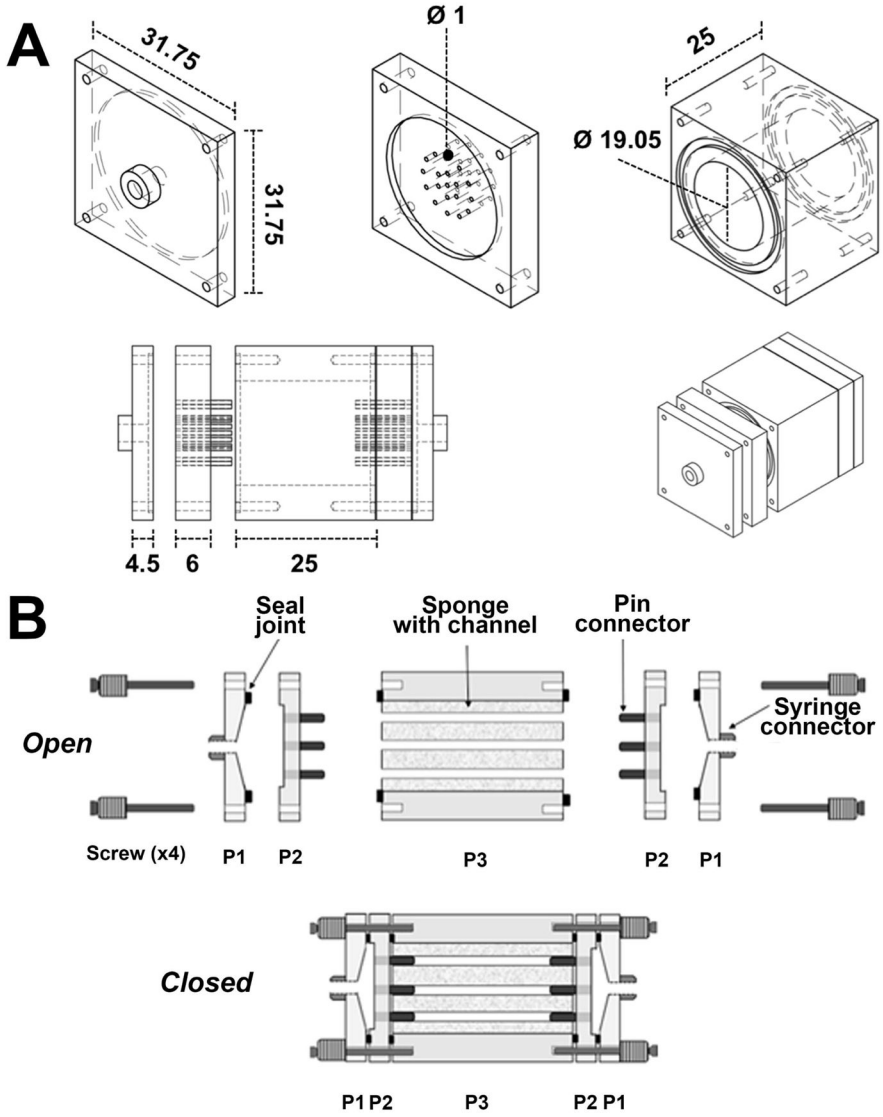

Fig. 4.

Schematics of the different bioreactor components (top) and assembly (bottom). Dimensions are reported in millimeters (A). Schematic representation of bioreactor assembly (B).

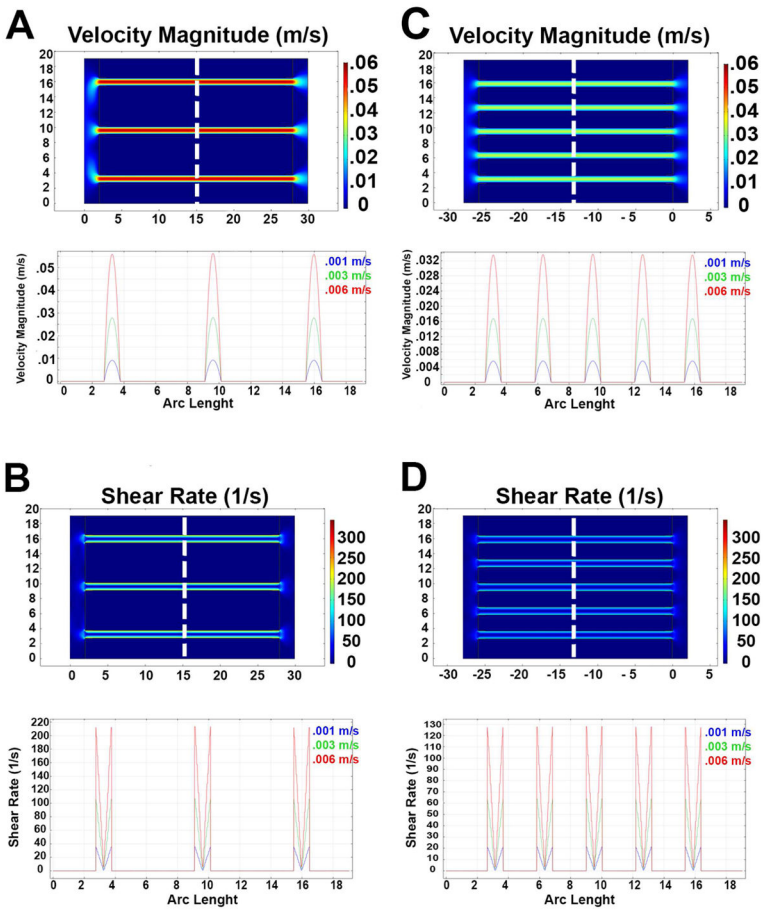

Fig. 5.

Flow velocity representation of the 7 and 13 channels scaffolds at 3 different flow input velocities (A–C respectively); the top panel shows the flow velocity distribution in the bioreactor's cross section at a flow input of 0.006 m/s. Flow direction left to right. The bottom panels show the flow velocity profile calculated at a fixed distance from the inlet (dashed line) at 3 different flow input velocities. Shear rate representation of the 7 and 13 channels scaffolds at 3 different flow input velocities (B–D respectively). The top panel shows the flow velocity distribution in the bioreactor's cross section at a flow input of 0.006 m/s. The bottom panels show the shear rate profile calculated at a fixed distance from the inlet (dashed line) at 3 different flow input velocities.

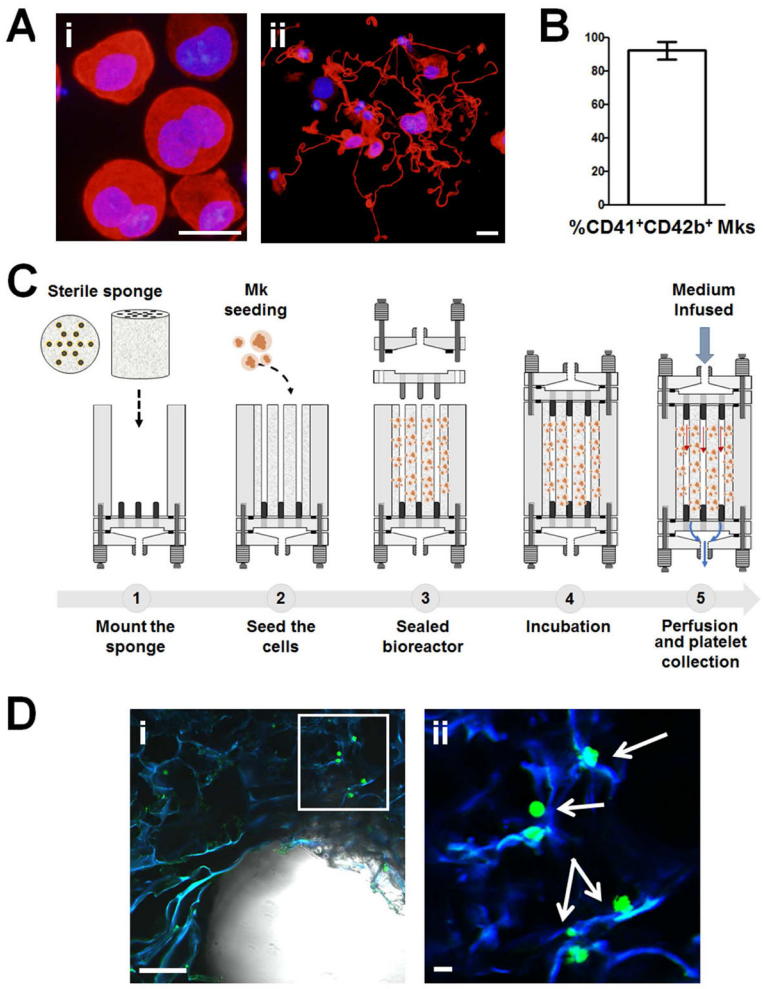

Fig. 6.

Representative immunofluorescence microscopy analysis of *in vitro* differentiated Mks from cord blood at day 13 of culture (red = β1-tubulin; blue = nuclei; scale bar = 25 μm) (Ai). Representative immunofluorescence analysis of proplatelet formation and structure from cord-blood derived Mks in adhesion on type IV collagen-coated glass coverslips (red = β1-tubulin; blue = nuclei; scale bar = 10 μm) (Aii). Percentage of $CD41^{+}CD42b^{+}$ *in vitro* differentiated Mks from cord blood hematopoietic progenitors (B). Schematic representation of 3D Mk culture (C). Representative confocal microscopy imaging of a lyophilized silk sponge upon $CFSE^{+}$ Mk seeding (scale bar = 200 μm) (Di). Greater magnification of the area contained within the white box highlighting Mks adhering onto silk scaffold. Arrows indicate $CFSE^{+}$ Mk (green = Mks; blue = silk; scale bar = 50 μm) (Dii)

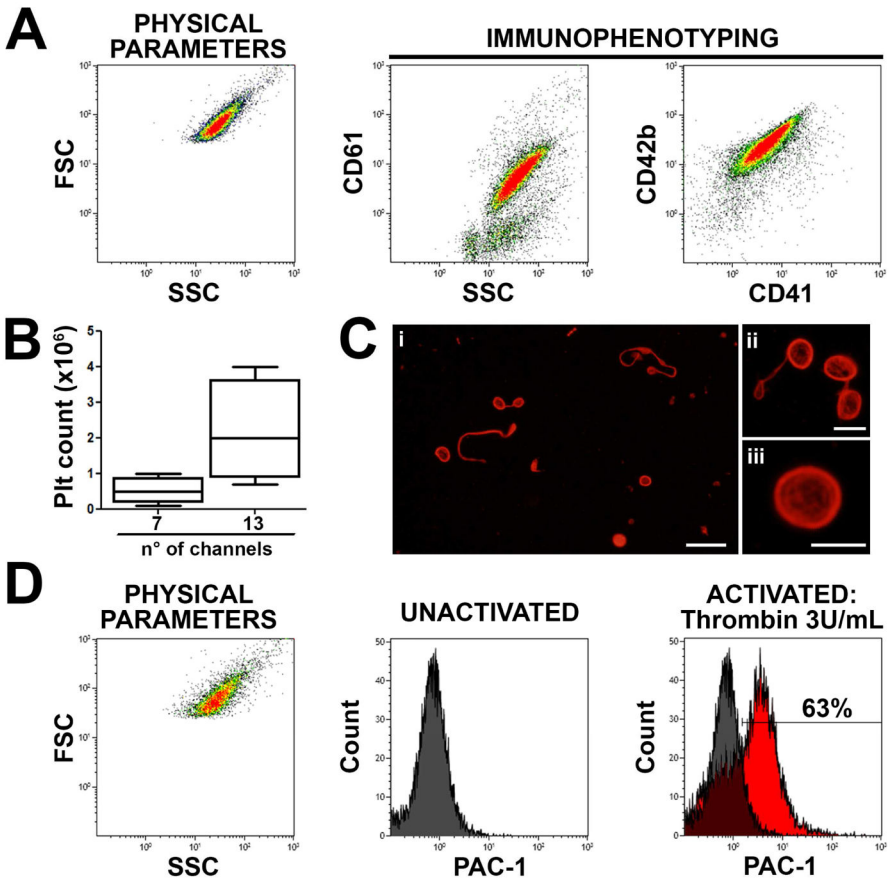

Fig. 7.

The sponge bioreactor was perfused with culture media for 6 hours and released platelets collected into gas-permeable bags. Flow cytometry analysis of expression of CD61, CD41 and CD42b surface markers by *ex vivo* produced platelets (A) and box count of platelet released by 7 or 13 channels-containing sponges (B). Microscopy analysis by immunofluorescence labelling of the β1-tubulin showing *ex vivo* produced platelets (red = β1-tubulin; scale bar = 10 μm) (Ci). Higher magnification highlight barbell proplatelet (red = β1-tubulin; scale bar = 3 μm) (Cii) and discoid platelet (Ciii) (red = β1-tubulin; scale bar = 3 μm). Flow cytometry analysis of collected platelet activation before and after treatment with 3 U/mL thrombin demonstrated increased PAC-1 binding indicating physiologic CD41 activation (D).